AD-A170 148 THEORY OF SPECTROSCOPY AND DYNAMICS IN LASER-IRRADIATED ADSPECIES-SURFACE (U) STATE UNIV OF NEW YORK AT BUFFALO DEPT OF CHEMISTRY T F GEORGE ET AL JUL 86 UBUFFALO/DC/86/TR-9 N00014-86-K-0043 F/G 7/4 NL

1/1

UNCLASSIFIED

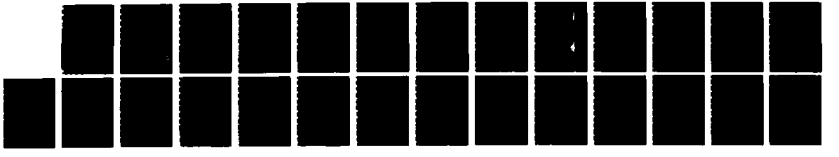

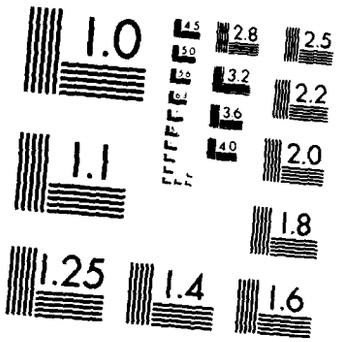

OFFICE OF NAVAL RESEARCH

Contract N00014-86-K-0043

TECHNICAL REPORT No. 9

Theory of Spectroscopy and Dynamics in Laser-Irradiated Adspecies-Surface Systems

by

Thomas F. George, Daniel Jelski, Xi-Yi Huang and A. C. Beri

Prepared for Publication

in

Interfaces under Laser Irradiation
edited by D. Bäurle, G. Dewel, L. D. Laude and M. Wautelet
M. Nijhoff Publishers, NATO Advanced Summer Institutes Series

Departments of Chemistry and Physics
State University of New York at Buffalo
Buffalo, New York 14260

July 1986

Interfaces under Laser Irradiation
Edited by D. Bäurle, G. Dewel, L. D. Laude and M. Wautelet
M. Nijhoff Publishers, NATO Advanced Summer Institutes Serie

THEORY OF SPECTROSCOPY AND DYNAMICS IN LASER-IRRADIATED ADSPECIES-SURFACE SYSTEMS

THOMAS F. GEORGE AND DANIEL JELSKI
Departments of Chemistry and Physics & Astronomy
239 Fronczak Hall
State University of New York at Buffalo
Buffalo, New York 14260 USA

XI-YI HUANG
Department of Chemistry
University of Rochester
Rochester, New York 14260 USA

A. C. BERI
Systems Sciences Division
Computer Sciences Corporation
Beltsville, Maryland 20705 USA

1. INTRODUCTION

Recent progress in the theory of spectroscopy and dynamics in laser-irradiated adspecies-surface systems is discussed. This article is divided into three main sections. Beginning with Section 2 following this Introduction, a first-principles approach for describing vibrational excitation and relaxation of a laser-excited adatom is presented. A tractable approximation, known as the isomnesic (constant-memory) approximation is introduced in order to numerically deal with the long-time behavior of the dynamics. In Section 3 surface-dressed optical Bloch equations are solved for the resonance fluorescence spectrum of a laser-driven two-level atom near a flat metal surface and also near a rough metal surface modeled by a hemispheroid on a perfectly conducting plane. In Section 4 the problem of laser-induced period chemical vapor deposition is addressed, and a theoretical analysis of selected aspects of an experiment on the deposition of cadmium onto a silica surface is carried out, where the cadmium is produced by laser-induced dissociation of dimethyl cadmium gas above the surface.

2. VIBRATIONAL EXCITATION AND RELAXATION

We describe here a first-principles approach, which is divided into four parts. Part 2.1 is a brief introduction to the Zwanzig formalism for dealing with non-Markovian phenomena and approximations which make the method capable of describing long-range chemical processes with memory effects. Part 2.2 is an application of the theory to a fictitious system chosen to best illustrate effects peculiar to resonantly laser-excited vibrational manifolds, especially effects resulting from selective laser photochemistry. In Part 2.3 the theory is applied to a "real" system -- hydrated atomic hydrogen on the KCl(001) surface -- and the results are extended to chemical reaction times. Finally, in Part 2.4 a desorption

channel is introduced, and important trends in the resulting desorption rate are discussed.

2.1. BASIC THEORY

The theoretical basis for the first-principles approach is the Heisenberg equation of motion

$$\dot{\rho}(t) = (i\hbar)^{-1}[H,\rho(t)] = -iL\rho(t) \quad , \tag{1}$$

where H is the Hamiltonian operator, L is the corresponding Liouvillian operator, and $\rho(t)$ is the density operator of the system. The Hamiltonian is partitioned into zeroth-order Hamiltonians for the solid and the adbond (the adspecies in the phonon-averaged field of all the lattice atoms) plus a perturbation representing the adbond-lattice interactions and another representing the adbond-laser interaction. Within the Born approximation and random-phase assumption, the equation of motion for an adatom-surface system leads to the generalized master equation (GME)[1]

$$\dot{P}_S(t) = \int_0^t dt' \left[\sum_{S' \neq S} K_{SS'}(t-t')P_{S'}(t') - \sum_{S' \neq S} K_{S'S}(t-t')P_S(t') \right] \quad , \tag{2}$$

which is an integrodifferential equation of the Volterra type. P_S is the occupation probability of the vibrational state $|s\rangle$ of the adbond, and the memory kernels $K_{SS'}$ incorporate the phonon (p) and the radiation (r) terms: $K_{SS'} = K^{(p)}_{SS'} + K^{(r)}_{SS'}$. For a Debye model of the solid, we have obtained the phonon portions $K^{(p)}_{SS'}$ in closed form,[2-4] and find them to be fairly complicated with a predominantly damped oscillatory behavior. Numerical solution of a Volterrra-type equation with a nonmonotonic kernel is very difficult.[5] In our case we were able to solve it only for $t \leq 5$ ps.[2] As a general rule, we have found that exact numerical solutions of the problem of vibration laser-adbond-surface energy transfer are possible only for times of the order of a few Debye periods (inverse of the Debye frequency, ω_D). This is hardly sufficient to describe chemical processes, so we have been studying possible techniques for overcoming this "non-Markovian bottleneck."

One such technique is based on a constant-memory approximation, i.e., isomnesic approximation (IA), to the memory kernel.[4] Briefly, the short temporal range of $K^{(p)}_{SS'}(t)$ suggests a delta-function representation if the long-time behavior (accurate beyond this temporal range) is of interest. Thus,

$$K_{SS'}(t) = \Omega_{SS'}\delta(t) + K^{(r)}_{SS'} \quad . \tag{3}$$

The second term on the right-hand side is time-independent. If it were a delta function also, we would obtain the Markovian approximation (MA). However, because of the constant terms $K^{(r)}_{SS'}$ we obtain instead a nonconvolution-type integrodifferential equation

$$\dot{P}_S(t) = \sum_{S'} K^{(r)}_{SS'} \int_0^t dt' \, P_{S'}(t') + \sum_{S'} \Omega_{SS'}P_{S'}(t) \quad , \tag{4}$$

which reduces to the following second-order differential equation (we note that the Markovian master equation is first order):

$$\ddot{P}_S(t) = \sum_{S'} K^{(t)}_{SS'} P_{S'}(t) + \sum_{S'} \Omega_{SS'} \dot{P}_{S'}(t) \quad . \tag{5}$$

We have found a convenient method for solving this based on Laplace transforms and the Heaviside expansion theorem.[6]

2.2. SELECTIVE PHOTOEXCITATION OF A PROTOTYPE SYSTEM

As a prototype system, we choose a mass 16 species on Ge which develops six bound states (S = 0,1,2,3,4,5) in the adbond potential. We also choose a situation where $|\omega_{10}| = \omega_D$ and $|\omega_{13}| = \omega_L$, where $\omega_{SS'}$ is the transition frequency between levels S and S' and ω_L is the laser frequency, so that the laser does not cause direct transitions between phonon states. The resulting population profiles are shown in Figure 1 for S = 0, 1 and 3 along with results of the exact numerical solution of the GME, Eq. (2). As expected, there is a loss in fine detail with the IA, but the average behavior is surprisingly well reproduced. Thus, for example, the crossing point where $P_1(t) = P_3(t)$ for the first time is at t = 1.7 ps in the IA as compared to t = 2.2 ps in the exact numerical solution. The relative behavior of P_0, P_1 and P_3 is also close to that obtained numerically.

Substantial chemical information is contained in the average adbond energy

$$\bar{E}(t) = \sum_{S} P_S(t) E_S \quad , \tag{6}$$

where

$$H_S|S\rangle = E_S|S\rangle \quad . \tag{7}$$

Figure 2 depicts $\bar{E}(t)$ obtained by solving the exact and isomnesic GME. We notice that the energy does not change monotonically, but consists of alternating influx and efflux. Figures 1 and 2 together display a feedback mechanism. Depletion of level S = 0 corresponds to energy transfer out of the phonon field, and we see such a depletion for $t \leq 5$ ps. This feedback is an important microscopic effect suggested in our earlier model calculation[7] but often missed in average statistical theories which examine only the long-time steady-state behavior of many-body systems. Figures 3 and 4, which show $P_S(t)$ and $\bar{E}(t)$ using the IA for 20 ps, further clarify the situation. The average energy content of the adbond is periodic, with an initial fast rise followed by a fall and subsequent smaller-amplitude damped oscillations. Between 0 and 4.8 ps, $P_0(t)$ decreases while $\bar{E}(t)$ increases; energy is transferred from the solid (and the laser, of course) to the adbond. However, subsequently between 4.8 and 7.7 ps, $P_0(t)$ increases while $\bar{E}(t)$ decreases, i.e., the phonon field is replenished at the expense of the adbond energy. But then again, the laser causes sufficient depletion of P_1 for phonon energy to get transferred back to the adbond, causing a depletion of P_0, which is energy feedback. The solutions of a Markovian version of this formulation

EXACT vs. *ISOMNESIC*

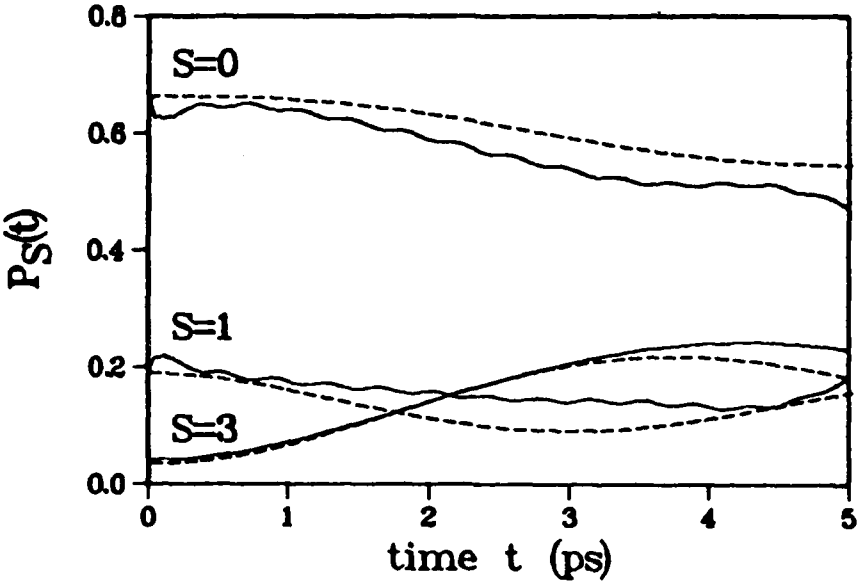

FIGURE 1. Probability profiles $P_S(t)$ for levels S = 0, 1 and 3 of the adbond. Solid lines: exact numerical solutions of the GME, Eq. (2); broken lines: closed-form solutions with the isomnesic approximation.

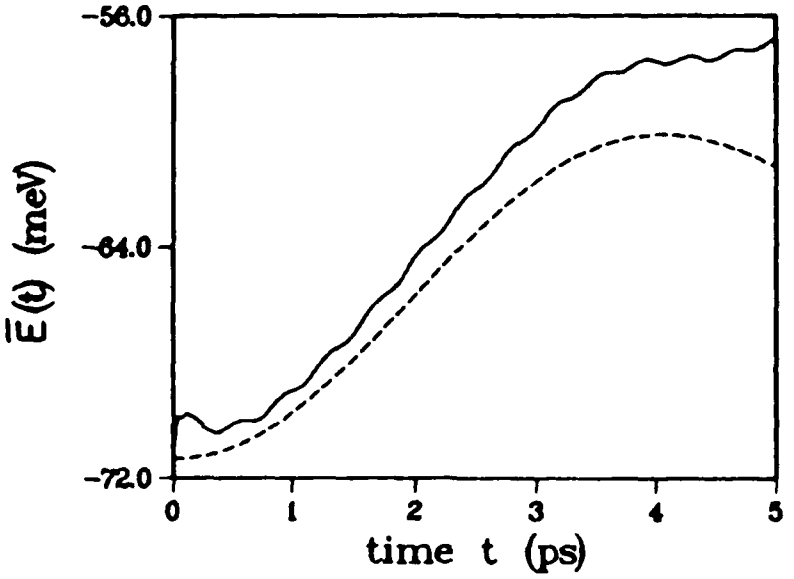

FIGURE 2. Average adbond energy $\bar{E}(t)$ obtained via the exact numerical solution of Eq. (1) (solid line) and closed-form solution with the IA (broken line).

ISOMNESIC vs. *MARKOVIAN*

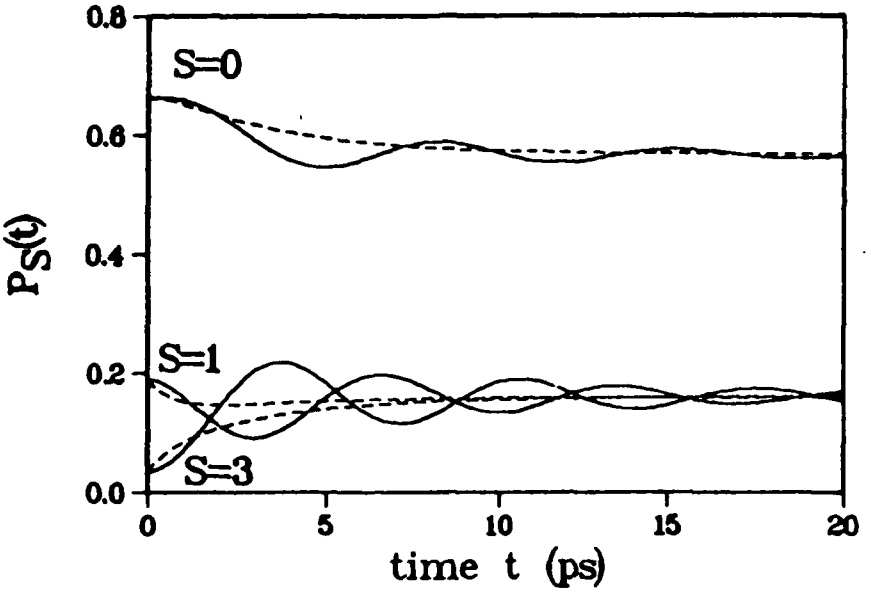

FIGURE 3. Comparison of $P_S(t)$ with the IA (solid lines) and the MA (τ = 1 ps; broken lines) for S = 0, 1 and 3.

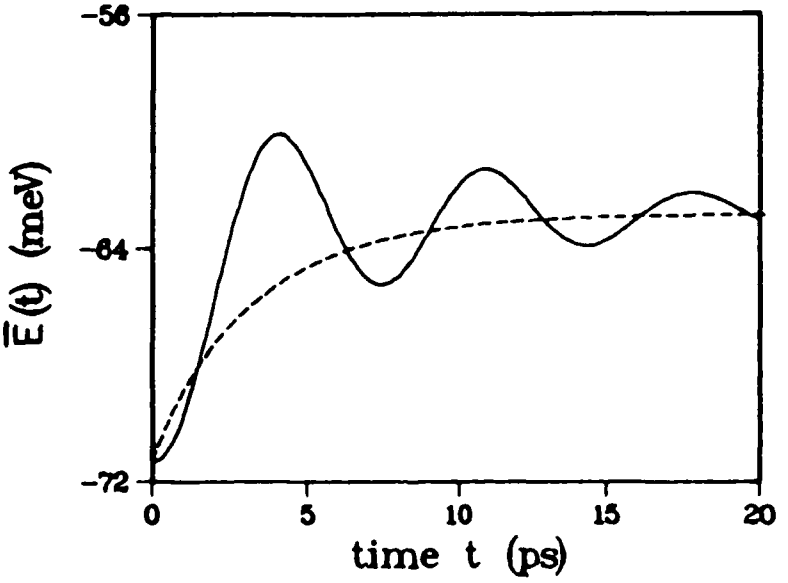

FIGURE 4. $\bar{E}(t)$ with the IA (solid line) and the MA (τ = 1 ps; broken line).

(obtained by replacing $K^{(r)}_{SS'}$ in Eq. (3) by $K^{(r)}_{SS'}\tau\delta(t)$, where τ is a time-range parameter) display no such feedback mechanism (broken lines in Figures 3 and 4).

The isomnesic approximation represents a significant improvement over the Markovian approximation and has definite advantages over the exact numerical treatment, since the IA is an analytic (nonnumerical) theory and is not subject to the time constraints inherent in the exact first-principles treatment. We are thus able to follow the time evolution of the adbond probability distribution for arbitrarily long times and to study the steady state. The Markovian limit is studied for the purpose of establishing a link between our new theory and the majority of past work on the chemical dynamics of many-body systems far from equilibrium. We find that such a (Markovian) treatment is inherently arbitrary and leads to qualitatively different results depending on the choice of the time-range parameter τ for the laser radiation.[4] Approach to equilibrium in the Markovian approximation is monotonic (a superposition of exponential changes), while the exact and IA treatments give rise to oscillatory behavior for the population distribution of the adbond. However, we do find that the steady state is the same for the IA and the MA. The important point here is that the IA is essentially as convenient and simple to work with as the MA, but gives results which are very faithful to the exact first-principles description of the phenomenon. We now proceed to applications of the above approach involving the IA.

2.3. LONG-TIME EFFECTS OF SELECTIVE PHOTOEXCITATION

Recent studies[8] have suggested that extremely high laser powers would be necessary to effectively desorb adspecies from a solid surface via a selective absorption mechanism. However, our recent work[3] has shown that a very small degree of detuning between the laser and energy levels of the system excludes the possibility of long-term energy absorption. The reason for this behavior is seen to be the oscillatory nature of the laser energy absorption "rate" (actually, the memory kernel) for the adbond, with a frequency related to the detuning, typically a small percentage of the laser frequency itself, namely $10^{10} - 10^{11}$ s^{-1}. Substantial cancellation in the overall absorption results and a very high laser power would be needed for the absorption to compete with phonon relaxation effects. In order to emphasize the special role of the coherence and monochromoticity of lasers in selective photoexcitation, a system with essentially no detuning has been chosen for the application of the isomnesic approximation to long time IR laser pumping.

Our formalism has been applied to the system $H(H_2O)/KCl(001)$,[9] where the primary reasons for choosing this are the shallow adsorption potential well and the small number of bound states (seven) it generates.[10] Figure 5 is a composite display of the function $\bar{E}(t)$ for six ranges of time differing by factors of 10 and for a laser intensity of 1 W/cm^2. It is seen that in going from a picosecond time range to a microsecond time range, the behavior of the system changes dramatically. The early behavior is dominated by fast energy transfer to phonon modes, completely overwhelming the slow laser pumping. The monotonic decay is representative of relaxation phenomena. For the 100 ps range, a false steady state seems to have been reached, but is in fact only an artifact of the large difference between the amplitudes of the laser and phonon kernels. The adbond energy starts to increase in the ns range, again

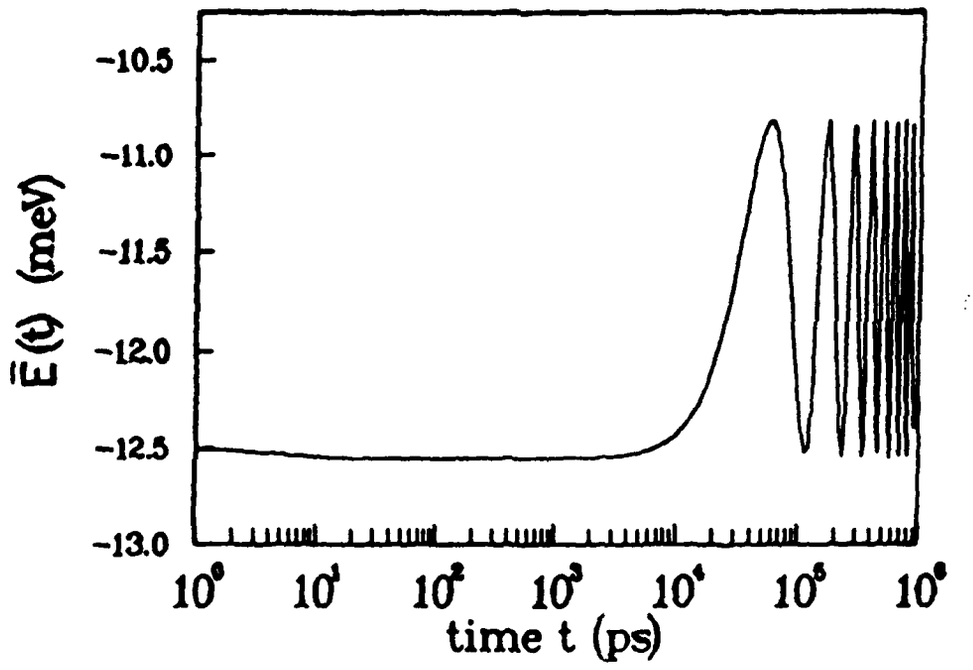

FIGURE 5. E(t) obtained by using the isomnesic approximation for time scales ranging from ps to μs for a laser intensity of 1 W/cm^2.

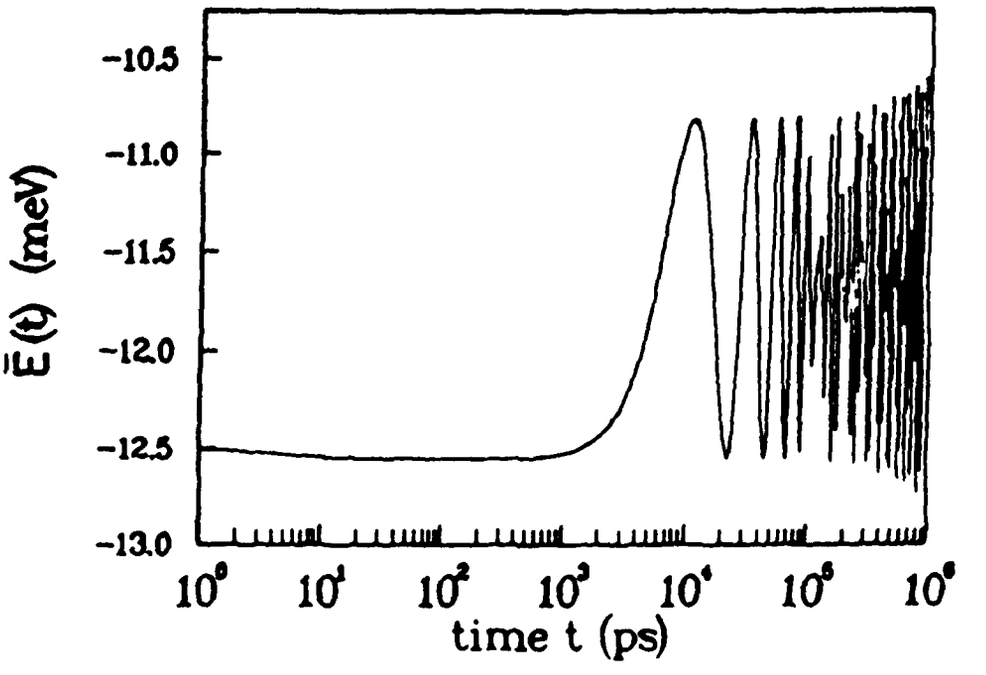

FIGURE 6. Same as Figure 5 for a laser intensity of 25 W/cm^2.

suggesting a possible steady state. However, this is a transitional period during which the relative importance of the phonon terms and the laser terms starts to change. The latter, in fact, originate from a probability profile of the form $(Ae^{\alpha t}\cos\beta t - \beta^{\alpha t}\sin\beta t)$, where $\alpha + i\beta$ are complex roots of det $\underline{M}(s) = 0$, and $A + i\beta$ are complex coefficients obtained from $\underline{M}(s)$ and $\vec{T}(s)$, where the matrix $\underline{M}(s)$ and the vector $\vec{T}(s)$ are related to the Laplace transform of the isomnesic master equation.

The phonon terms come from real roots and are therefore nonoscillatory. The magnitudes of the exponents α in the laser part of the solution are much smaller than corresponding exponents in the phonon term. This is responsible for the radically different nature of $\bar{E}(t)$ in the different time regimes. Thus, the seemingly monotonic rise in $\bar{E}(t)$ apparent in the 10 ns regime is seen to be only the early segment of a cycle which becomes evident in the 100 ns results and beyond. The frequency of this oscillation is seen to be $K_0^{1/2}$, where K_0 is the amplitude of the laser kernel $K_{SS'}$, and is essentially the Rabi frequency for the pair of levels resonant with the laser.

While the frequency of the long-term oscillations of $P(t)$ and $\bar{E}(t)$ depends only on the laser term, being proportional to the square root of the intensity, the rate of onset of this behavior depends on α which varies linearly as K_0 and inversely as the amplitude Ω_0 of the phonon kernel. Thus, increasing the laser intensity from 1 to 25 W/cm^2 advances the onset time for the oscillatory state while increasing the frequency by a factor of 5 (as displayed in Figure 6).

Physically the results of Figures 5 and 6 can be interpreted in terms of desorption rates. Thus the time required for $|A|e^{\alpha t}$ and $|\beta|e^{\alpha t}$ to become large enough, so that the amplitude of $E(t)$ in the oscillatory regime is substantially larger than the $(t = 0)$ equilibrium Boltzmann value, is a reasonable measure of the desorption time to within an order of magnitude. This time is estimated by $\tau_D = \alpha^{-1}$. For our case,

$$\tau_D^{-1} = \alpha \cong 0.5\,\frac{K_0}{\Omega_0} \cong (10^4\ I)s^{-1} \quad , \tag{8}$$

where w is the laser intensity in W/cm^2. Thus, for a 1 W/cm^2 laser, a hydrogen atom will stay adsorbed on the KCl(H_2O) surface for $\sim 10^{-4}$ s on the average before desorbing, or at least becoming very highly excited. The data mentioned here is for T = 150 K.

It must be pointed out that a number of mechanisms whereby the desorption cross section could be modified are not included. Spontaneous decay, phase relaxation, phonon-phonon interaction and electron-hole pair creation are some of the ones being considered in extensions of this work. As a result, the sharp transitions assumed here will be broadened by a detuning-type effect, and estimates of the desorption rate presented above will have to be modified. However, the selectivity represented by the dominant T_1 energy-transfer process will be retained.

2.4. DESORPTION

Desorption is the most commonly studied phenomenon of laser-stimulated surface processes, and recent experiments[11-13] have shown a strong dependence of the desorption cross section on the laser frequency. While energy transfer during IR-laser stimulated surface processes has been discussed for the above work in the absence of a desorption channel,

selective absorption has been demonstrated for vanishing mismatch between the laser and adbond frequencies. The time-dependent energy profiles for the adbonds showed an initial strong increase followed by a decrease (transfer to bulk phonons) and, subsequently, another rise due to feedback from the phonons. We now present the results of an isomnesic formulation including desorption in the form of a transition from an excited state of the adsorption potential to the continuum.[14]

Let us consider a three-level system -- $|S\rangle = |0\rangle$, $|1\rangle$ and $|3\rangle$ -- one of whose transitions is resonant with the laser, and another equals the phonon Debye frequency. In the absence of desorption, application of the Laplace transform method to the GME leads to a third-order polynomial equation. With the inclusion of a depletive desorption channel, the GME reduces to a quartic. As expected, the <u>total</u> population for the adbond is depleted monotonically, and the desorption probability $P_D(t)$ grows correspondingly to a maximum value $P_T(0)$. The average adbond energy $\bar{E}(t)$ increases with time, but because of the competition between laser pumping and desorption, the detailed behavior of the energy profile is not as simple as that of $P_D(t)$. Depending on the magnitude of the bound-to-continuum transition rate R, $\bar{E}(t)$ has a monotonic (nonoscillatory), sigmoid profile which is is an oscillatory profile akin to the nondesorptive behavior, or a transitional profile. For 10^{-16} ps^{-1} $\leq$ R $\leq$ 1 ps^{-1}, both the cessation of slow oscillatory behavior and the onset of fast sigmoid behavior take place at higher laser powers for larger values of R. The trends observed are important from the point of view of selective laser photochemistry. Thus, for a given value of R, laser powers falling in the oscillatory region will cause a very slow accumulation of vibrational energy in the adbond, while laser powers falling in the transitional or sigmoid regions will excite the adbond quickly and cause almost instantaneous desorption.

3. RESONANCE FLUORESCENCE OF A TWO-LEVEL ATOM NEAR A METAL SURFACE

The lifetime of an excited molecule has experimentally been found to vary dramatically as a function of distance from a metal surface.[15] A number of researchers have examined this effect from the viewpoint of reflected-field theory, where the basic calculation is concerned with the interaction between an excited molecule and its own reflected radiation field. This theory generally provides good agreement with experiments.[15-26]

When an adatom is driven by strong resonant, driving coherent field, it creates for the atom or molecule an environment where the probability of stimulated emission can exceed that of spontaneous emission. Under this condition, dynamic ac-Stark splitting and nutational oscillation of the emitted light intensity become important parts of the laser-driven processes, such that interesting "resonance fluorescence" and other nonlinear optical phenomena can occur.[27] We have recently derived a set of surface-dressed optical Bloch equations,[21-26] by which we can examine the dynamics and relaxation of an adatom near a metal surface. By solving these equations, we have been able to evaluate the resonance fluorescence spectrum of a two-level atom near a metal surface, taking the following factors into account:

(i) the reflected electromagnetic field effects due to the presence of the interface
(ii) collision dephasing

(iii) surface-induced dephasing due to reflected photons
(iv) resonance excitation of surface plasmons
(v) random-phase fluctuations of the laser.

Besides these studies, we have been extending the flat-surface resonance fluorescence calculations to the rough surface case, which is modeled as a hemispheroidal protusion on a perfectly-conducting surface.[26] We discuss our progress below.

Let us begin with the case of a flat metal surface and the set of surface-dressed optical Bloch equations (SBE), which include the effect of surface-reflected photons, i.e., photons emitted by the laser-driven atom and reflected by the surface.[21,22] Within the rotating-wave approximation the SBE take the form

$$\frac{d}{dt}\begin{pmatrix}\hat{S}_{21}(t)\\ \hat{W}(t)\\ \hat{S}_{12}(t)\end{pmatrix} = \begin{pmatrix}-\tilde{\gamma}_2+i\Delta & i\Omega^-(t)/2 & 0\\ i\Omega^+(t) & -\gamma_1 & -i\Omega^-(t)\\ 0 & -i\Omega^+(t)/2 & -\tilde{\gamma}_2-i\Delta\end{pmatrix}\begin{pmatrix}\hat{S}_{21}(t)\\ \hat{W}(t)\\ \hat{S}_{12}(12)\end{pmatrix} - \gamma_1\begin{pmatrix}0\\1\\0\end{pmatrix}, \quad (9)$$

where $\hat{W} = |2><2| - |1><1|$ is the population inversion of the atom, $\hat{S}_{ij}$ is product of $\exp(i\omega_L t)$ and the transition operator $|i><j|$, $\Omega^{\pm}(t)$ is the time-dependent Rabi frequency, $\Delta = \omega_{21} - \omega_L$ is the detuning of the laser (ω_L) with respect to the two-level atom (ω_{21}), and the dephasing rate constant $\tilde{\gamma}_2$ is the sum of the radiative dephasing γ_2 and the surface-induced dephasing γ_s. The driving and reflected fields are treated semiclassically, and we assume the atom-surface distance to be large ($\gtrsim 30$ nm). The relaxation time included in the Drude model for the complex dielectric constant of the metal medium represents the dissipation of electron gas which, together with surface plasmon resonances, influences the surface reflectivity and hence the behavior of the reflected field. Here we may neglect nonradiative transfer of energy from the excited atom to the metal. Effects of the laser bandwidth are included by means of a phase diffusion model for the driving field. In the weak-field or large-detuning limit, the power spectrum of scattered light has two peaks: one corresponding to Rayleigh scattering at the laser frequency ω_L and the other to fluorescence at the atomic transition frequency ω_{21}. For a sufficiently strong driving laser field, the spectrum exhibits three peaks: a central one at $\omega_0 = \omega_L$ (Rayleigh component), a left one at $\omega_- = 2\omega_L - \omega_{21} - \delta$ (three-photon component) and a right one at $\omega_+ = \omega_{21} + \delta$ (fluorescence component), where δ is the ac-Stark shift.

Results for the peak heights H_-, H_0 and H_+ are shown in Figure 7 for the case of a silver surface.[22] The key feature, which is a unique behavior due to the surface, is that for certain atom-surface distances H_- is larger than H_+, whereas in the pure gas-phase resonance fluorescence spectrum H_- is always less than H_+ (due to molecular collisions for positive detuning). Also, the population inversion of the adatom and the resonance fluorescence spectrum, as well as the surface-induced phase-decay constant of the adatom, show strong oscillatory behavior as a function of the adatom-surface distance.[21,22]

For a rough surface, let us consider a surface protusion modeled by a prolate hemispheroid on top of a plane.[28,29] We note that this model has been shown to be identical to a full spheroid in a vacuum,[30] so that our calculations can also be used for an ellipsoidal cluster. The two-level

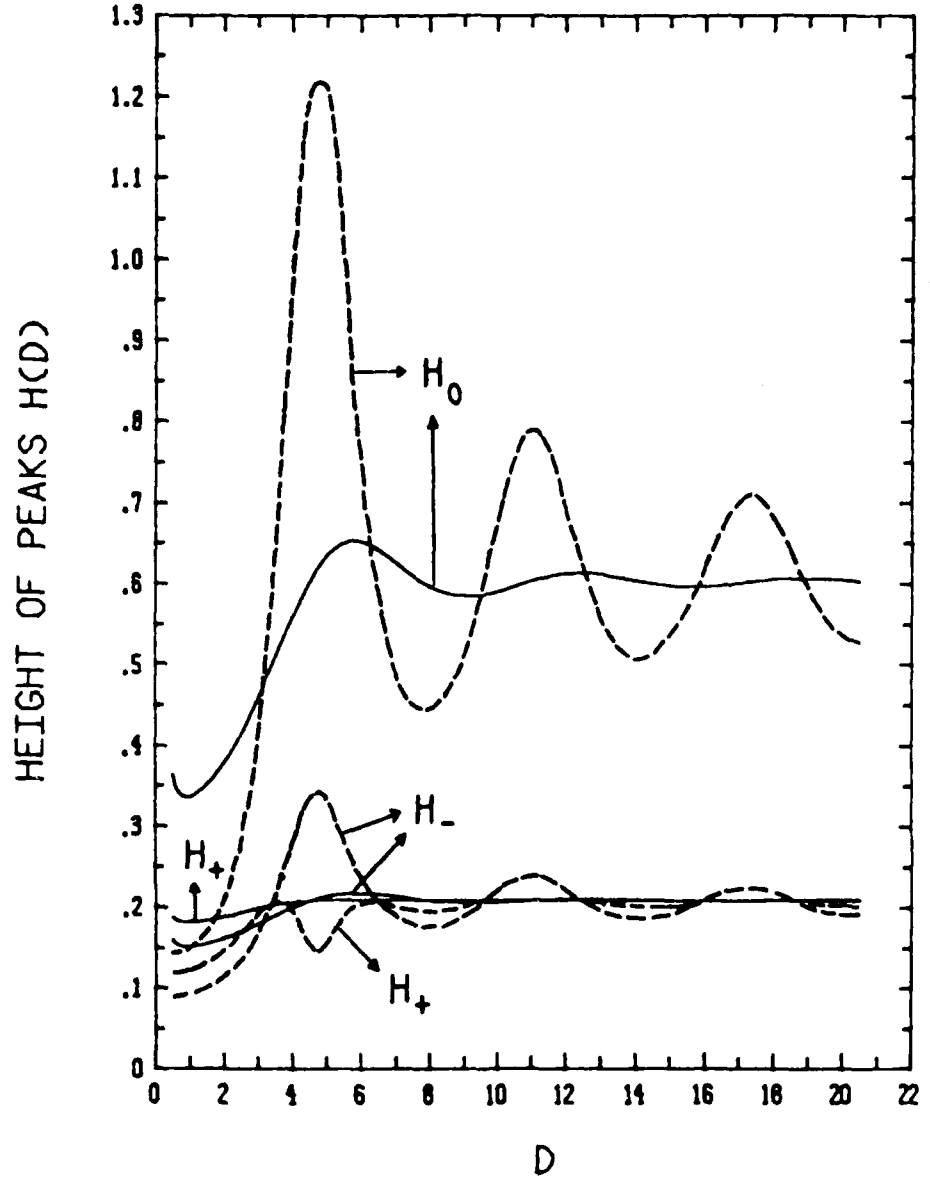

FIGURE 7. Atom-surface distance dependence of the heights of the three peaks in the resonance fluorescence spectrum for the case of a silver surface, where H_-, H_0 and H_+ correspond to the peak heights (in arbitrary units) of the three-photon, incoherent Rayleigh and fluorescence components, respectively. $D = 2kd$ is the reduced distance, where k is the wavenumber and d is the atom-surface distance. The Drude model is used for the dielectric function of the metal, while the dielectric function of the gas medium is set equal to one. The detuning $\omega_{21} - \omega_L$ is 1 A and the Rabi frequency is 10 A, in the unit of Einstein's A coefficient. The solid curves are for the induced transition dipole of the atom oriented perpendicular to the surface, and the dashed curves are for the parallel case.

adatom, which is located at a distance d from the top of the hemispheroid, is driven by a laser. The prolated spheroidal coordinates (ξ,η,ϕ) are used to calculate the reflected field. We define $\xi_1 = (a + d)/f$, $\xi_0 = a/f$ and $f = (a^2 - b^2)^{1/2}$, where a and b are the semi-major and semi-minor axes of the hemispheroid. The reflected field at the position of the adatom (transition dipole) in the near-field approximation can be written as[26]

$$E_r = -\frac{1}{f}\sum_n{}' C_n Q_n'(\xi_1) + \frac{\mu}{4(f\xi_1)^3} \quad , \tag{10}$$

where Q_n denotes the Legendre function of the second kind and μ is the induced dipole moment. The expansion coefficient C_n depends on the laser amplitude E_0 and parameters ξ_0 and ξ_1.[12] Based on the surface-dressed optical Bloch equations[21,22] appropriate for the excitation and dissipation of a two-level adatom near a hemispheroid, we find the surface-induced phase relaxation constant γ_s to be given by[26]

$$\gamma_s = (2/\hbar)\mathrm{Im}(F) \quad , \tag{11}$$

where

$$F = \frac{1}{1-\Gamma}\left[\frac{(1-\varepsilon)\xi_0 Q_1'(\xi_1)}{\varepsilon Q_1(\xi_0) - \xi_1 Q_1'(\xi_0)} + \Gamma\right] \quad . \tag{12}$$

Here ε is the complex dielectric constant, and Γ is a somewhat complicated function of ξ_0, ξ_1 and ε.

A sharp resonance enhancement of the adatom-hemispheroid interaction, through the reflected field at the atomic site, occurs when the specific shape of the prolate hemispheroid corresponds to a resonant excitation of plasmons (see Figure 8). The time oscillation of the level population decreases as the shape of the hemispheroid approaches the plasmon resonance. We also find that the strong-field three-peak fluorescence spectrum is strongly influenced by the roughness of the surface. The resonance excitation of the plasmon in the hemispheroid remarkably enhances the adatom-surface coupling, such that the dephasing processes broaden the linewidths of the spectrum. In the small detuning case, the spectrum has a distinctive three-peak nature, where the three-photon side peak has a measurable height which is almost comparable to the fluorescence side peak. The plasmon and reflected-field broadening influence equally the three spectral peaks. In the large detuning case, the height of the three-photon peak is decreased, and the three-peak spectrum is transformed to the weak-field two-peak structure.

4. LASER-INDUCED PERIODIC CHEMICAL VAPOR DEPOSITION

We have been engaged in theoretical research to explain laser-induced periodic vapor deposition recently observed experimentally.[31] While some pieces of the puzzle remain unsolved, we think that we now have a sufficient understanding of the phenomena to warrant a more general discussion.

Briefly, the experiment[31] which we are attempting to model is as follows. A dilute organometallic gas ($Cd(CH_3)_2$ in this case) is placed above a silicon or silicon oxide surface. The system is illuminated with

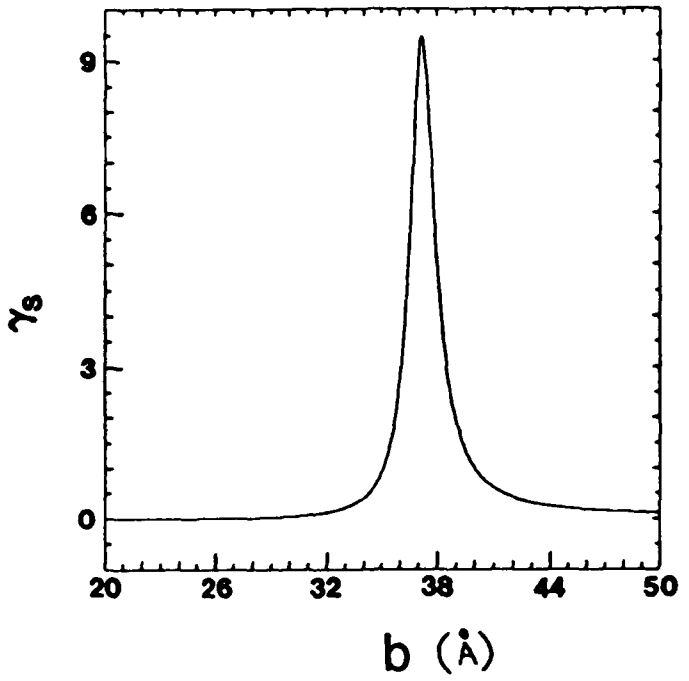

FIGURE 8. Rough surface-induced phase-decay constant γ_s as a function of the semi-minor axis b of the surface protusion, where the semi-major axis is fixed at 100 Å. γ_s is in the unit of Einstein's spontaneous decay constant A.

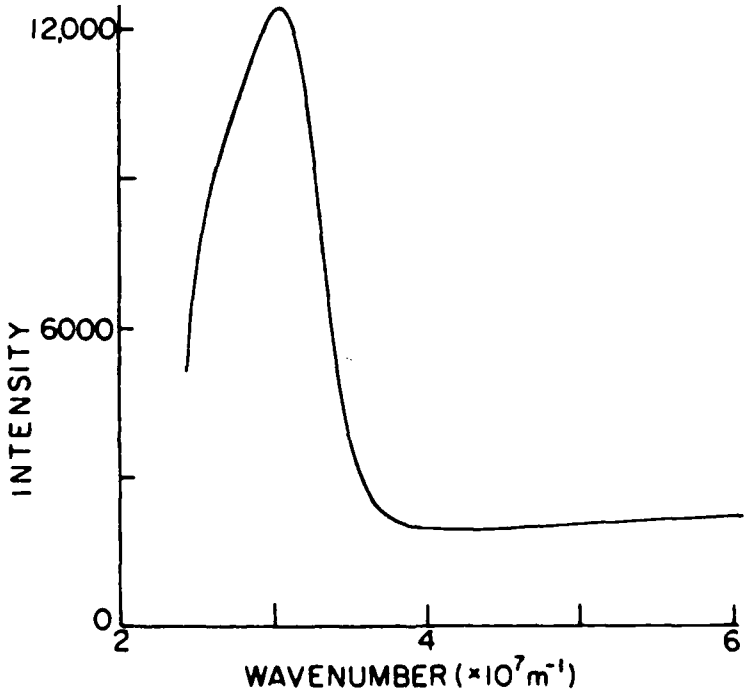

FIGURE 9. Graph of the plasmon field intensity as a function of grating wavenumber. The grating height is 25 nm, and 15 terms are kept when evaluating the modified Bessel functions.

a UV laser (257 nm) at low intensity (~ 10 W/cm^2). This dissociates the organometallic to a metal radical (in this case, cadmium), which is deposited on the surface. Deposition occurs evenly to a depth of about 200 nm, after which the deposition is periodic, with ripples developing in the p-polarized direction and growing to an added height of about 100 nm. In addition, much smaller ripples are formed in the s-polarized direction. This structure is very distinct and readily visible under a scanning electron micrograph.

The original experimenters, Brueck and Ehrlich,[31] postulated that the laser induces a plasmon field on the surface, where the varying field strength leads to the observed periodic deposition. They assumed the deposition rate to be proportional to the plasmon intensity, and using a first-order theory,[32] they showed that the plasmon field intensity is proportional to the grating height. It is therefore easy to conclude that the grating growth is exponential for shallow gratings.

We accept Brueck and Ehrlich's hypothesis as the starting point for our own work. Their discussion raises the following questions, some of which we shall be able to answer in this article:

1) What is the mechanism by which the plasmon enhances the deposition process? This is the major piece of the puzzle which remains unsolved, but we have more to say about this later.

2) What is the sequence of events in this experiment? Is the organometallic molecule dissociated in the gas phase, with deposition of the cadmium atom occuring later, or is the molecule physisorbed onto the surface, with dissociation occuring afterwards, perhaps as part of the chemisorption reaction of cadmium with the surface?

3) What is the dynamics of grating growth, and why does the grating stop growing? This last question is the one about which we now have the clearest understanding. We continue to work on the first two problems and shall discuss them in due course.

By accepting Brueck and Ehrlich's hypothesis that the grating growth is proportional to the strength of the plasmon electric field, then in order to derive a more precise expression for the dynamics, we must solve for the electric field above a rough surface. It is possible to do this numerically as accurately as required, but in order to gain some physical insight into the problem, we make two key approximations[33] which permit us to write an analytical expression for the growth rate:

1) We assume the Rayleigh hypothesis, namely that the solutions to the homogenous Helmholtz equation, which are exact above the selvedge region, are also valid within the selvedge region. This holds strictly only in the limit as the grating is infinitely shallow. How valid this approximation is depends on the precise nature of the mechanism by which the deposition occurs. We note that the gas pressure is about 1 torr, which means that the mean free path of the molecules is on the order of a millimeter, much longer than any grating height measured in the experiment. Thus if the relevant forces involved are long-range, most of the "action" takes place well above the selvedge region where our solution is exact, and we can use the Rayleigh hypothesis with impunity. On the other hand, if the mechanism is short range, then this introduces some uncertainty into our result, but we still expect to be able to qualitatively account for the phenomena.

2) Our second and more important approximation is the manner in which we truncate the Fresnel matrix. Toigo, Marvin and Celli[34] derived uncoupled equations for the electric field strength above a grating (given

the Rayleigh hypothesis), and their result has been used by many other researchers.[35,36] In principle, it is necessary to solve an infinite number of equations for an infinite number of unknowns, the unknowns being the amplitudes of the various order plasmons and/or Bragg reflections. Maradudin[34] has used this expression to derive the dispersion relation for a shallow grating. He did this by 1) assuming that the grating is shallow, and therefore only terms to first order in grating depth need be retained, and 2) that because the resonance condition is met, all field strengths are small relative to the resonance plasmon. This means that we can neglect all other reflections, and our infinite set of coupled equations reduces to two equations, easily soluble analytically.

Our contribution to this result is to notice that Maradudin's first assumption is unnecessary. If the resonance condition is met, then the resonance plasmon will be orders of magnitude larger than the other reflections, and hence we are justified in keeping all orders of the grating depth. This is true, of course, only as long as the resonance condition is met, but it implies that we can extend Maradudin's work to the deep grating case.

The implications of our approximation are best illustrated by studying Figure 9, where the x-axis is the grating wavenumber and the y-axis is the intensity of the plasmon field. Throughout we are insisting that the grating depth be 25 nm. Thus as the wavenumber becomes larger, the grating period becomes shorter, and the relative grating height becomes larger. Hence we see an increase in the plasmon field intensity, consistent with the previous result that the plasmon field increases linearly with grating height. The difficulty here is that this increase appears far from any resonance. Hence our approximation means that the two terms that we are keeping are on the same order of magnitude as the terms that we are dropping. This leads to a monotonically increasing function for the plasmon field strength, when in reality the curve would have more structure and would tend to approach some asymptotic value. In summary, for grating frequencies off resonance, our approximation over-estimates the plasmon field. Later we shall provide some measure for the degree of this error.

At resonance, on the other hand, the situation is different. Here the two terms that we are keeping are much larger than any others. Thus our approximation, while still tending to over-estimate the field strength, is much more accurate. Figure 10 illustrates the results of our method for various grating heights. Note the structure in the curves for gratings 15 nm and 20 nm deep. We suggest that this is physically reasonable since the resonance is very large, and the two terms we keep are quite complicated functions. On the other hand, our result for the 40 nm deep grating is suspect since there is no resonance whatsoever. In all cases we have kept 15 terms in evaluating the Bessel functions that appear in the equations.

Given the assumption that the grating growth rate is proportional to the plasmon field intensity, we are now in position to calculate the growth dynamics. Two problems are now presented. First, until we have a better knowledge of the mechanism by which the plasmon increases the growth, it is impossible to calculate the proportionality coefficient. Therefore, in our calculation shown in Figure 11, we have simply chosen the coefficient to match the time-scale of Brueck and Ehrlich's experiment. We are considering several possible models to explain this mechanism, and these will be discussed shortly.

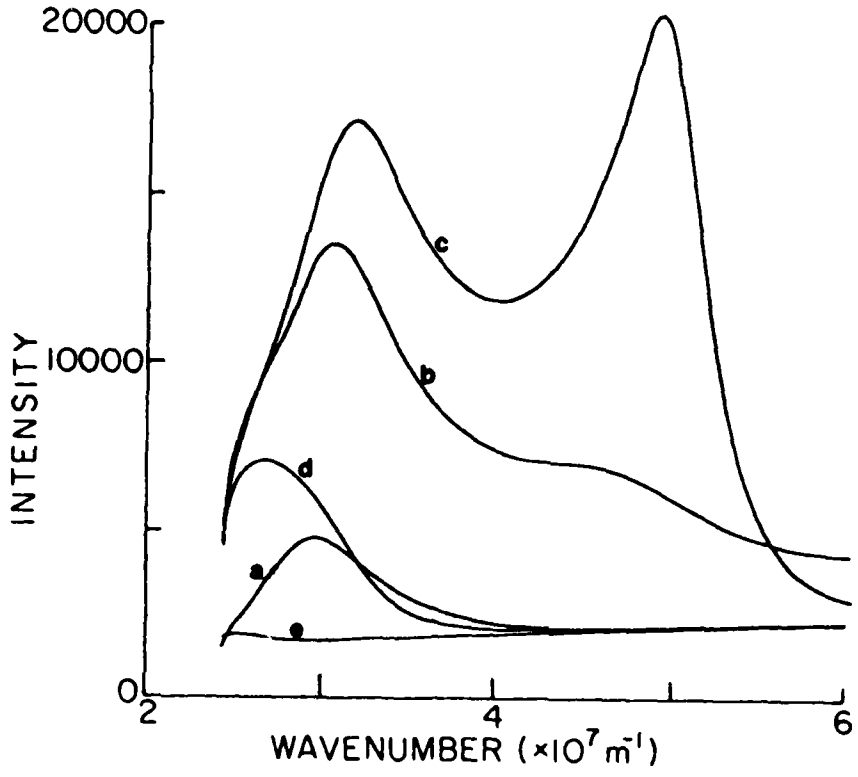

FIGURE 10. Same as Figure 9, except that the grating height is varied: (a) 5 nm, (b) 10 nm, (c) 20 nm, (d) 30 nm and (e) 40 nm.

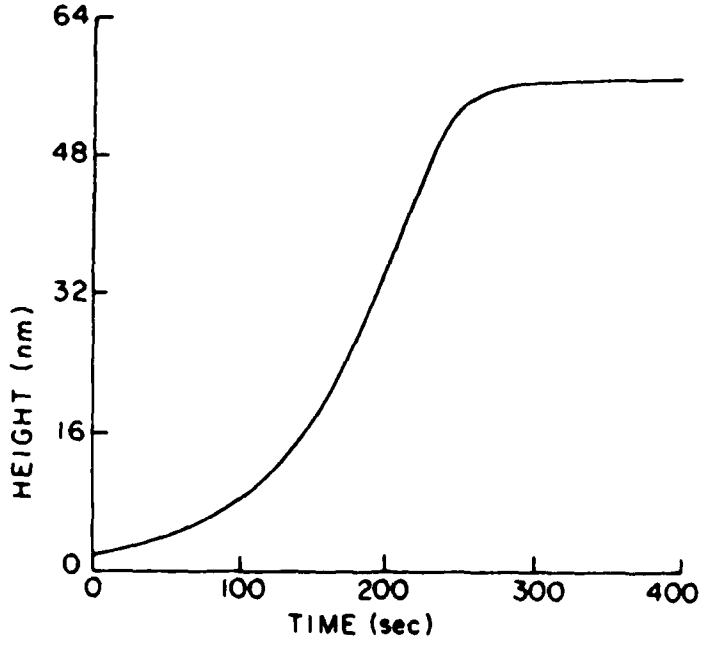

FIGURE 11. Grating height vs. time, calculated as described in the text.

The second problem is to determine when the grating stops growing. This happens when the resonance disappears altogether, and gratings of all frequencies grow at the same rate. Thus we have to subtract the "baseline" from the plasmon field intensity, namely the average intensity of all other plasmon frequencies. We have done this by treating the wavenumber of the light as the "base" wavenumber. This value is the left-most point of the curves shown in Figure 10. The reason for choosing this wavenumber is that it can never be at resonance since the laser-induced plasmons must oscillate at a wavenumber greater than that of the light. However, our approximation over-estimates the intensity of these off-resonant wavenumbers, so that we shall under-estimate the final peak height. This is shown in Figure 18, where the peak is shown growing to about 56 nm. Brueck and Ehrlich measure their peaks at about 100 nm. The discrepancy here gives us an indication of the accuracy of our approximations. If a method can be determined for calculating the "baseline" independently of our present model, which is obviously not valid for off-resonant wavenumbers, then we should be able to more accurately predict the maximum peak height.

Our discussion so far has revolved around the third of the three questions raised at the beginning of this article. We would now like to briefly discuss the other two. We have considered several possibilities for the mechanism by which the plasmon increases the deposition rate. The first, which at one point we considered most likely, is that the plasmon field induces a dipole in the adatom/molecule, which in turn attracts it to the surface. Unfortunately, the growth rate resulting from this mechanism is about 15 orders of magnitude too slow, and hence it is discarded.

A second possibility is that a charge transfer occurs between the surface and the cadmium atom, and hence the plasmon interacts with an ion and not a dipole. This appears to yield a growth rate on the right order of magnitude, but it remains unclear how the charge transfer takes place. It is conceivable that the plasmon field enhances the charge transfer process also, in which case a rate proportional to the square of the intensity is not impossible.

Yet another possibility is that the existence of the plasmon radically alters the shape of physisorption/chemisorption potential well. This raises the possibility that the growth is not proportional to the electric field intensity, but rather to the electron distribution along the surface. The very complexity of this problem forces us to exclude it from immediate consideration.

Finally, there is the dynamics of the dissociation process. We have reason to believe that this occurs in the gas phase, well above the surface.[37] If this is indeed true, then the problem becomes considerably simpler since the rate would depend only on the partial pressure of cadmium in the gas phase. We could then separate the problem into two parts: the gas-phase problem, i.e., the production of cadmium atoms, and the deposition problem. Depending on the pressure of the gas, one or the other will predominate in the total rate equation.

This concludes our discussion of recent progress made in the explanation of the periodic deposition phenomena. It only remains to make a few brief comments concerning the possible applications of such a model. An obvious question of interest would be how one could maximize either the grating height or growth rate. The development of a simple model will make it possible to predict ways to do this. Similarly, it may be

possible to change the deposition pattern by changing the parameters of the experiment. The calculation of this phenomenon involves more than what we have discussed here.

ACKNOWLEDGMENTS

This research was supported by the Air Force Office of Scientific Research (AFSC), United States Air Force, under Contract F49620-86-C-0009, and the Office of Naval Research. The United States Government is authorized to reproduce and distribute reprints notwithstanding any copyright notation hereon.

REFERENCES

1. A. C. Beri and T. F. George, J. Chem. Phys. 78, 4288 (1983).
2. A. C. Beri, K. T. Lee and T. F. George, in Proceedings of the International Conference on Lasers '83 ed. by R. C. Powell (STS Press, McLean, Virginia, 1985), pp. 362-369.
3. A. C. Beri and T. F. George, J. Chem. Phys. 83, 2482 (1985).
4. A. C. Beri and T. F. George, Z. Phys. B 60, 73 (1985).
5. See, for example, C. T. H. Baker and G. F. Miller, Eds., Treatment of Integral Equations by Numerical Methods (Academic Press, New York, 1982); L. Collatz, The Numberical Treatment of Differential Equations (Springer-Verlag, New York, 1966), Chapt. VI.
6. E. Butkov, Mathematical Physics (Addison-Wesley, Reading, Massachusetts, 1968), Chapt. 5.
7. J. Lin, A. C. Beri, M. Hutchinson, W. C. Murphy and T. F. George, Phys. Lett. 79A, 233 (1980).
8. C. Jedrzejek, K. F. Freed, S. Efrima and H. Metiu, Surf. Sci. 109, 191 (1981).
9. A. C. Beri and T. F. George, J. Vac. Sci. Technol. B 3, 1529 (1985).
10. H. Frank, H. Hoinkes and H. Wilsch, Surf. Sci. 63, 121 (1977).
11. J. Heidberg, H. Stein and E. Riehl, Phys. Rev. Lett. 49, 666 (1982).
12. T. J. Chuang and H. Seki, Phys. Rev. Lett. 49, 392 (1982); T. J. Chuang, J. Chem. Phys. 76, 3828 (1982).
13. T. J. Chuang, Surf. Sci. Rep. 3, 1 (1983).
14. A. C. Beri and T. F. George, J. Chem. Phys., submitted.
15. See the review by R. R. Chance, A. Prock and R. Silbey, Adv. Chem. Phys. 37, 1 (1978).
16. M. R. Philpott, Chem. Phys. Lett. 19, 435 (1973).
17. H. Morawitz, Phys. Rev. 187, 1792 (1969).
18. R. R. Chance, A. Prock and R. Silbey, J. Chem. Phys. 60, 2744 (1974).
19. K. H. Drexhage, J. Lumin. 1/2, 693 (1970).
20. H. Kuhn, J. Chem. Phys. 53, 101 (1970).
21. X. Y. Huang, J. Lin and T. F. George, J. Chem. Phys. 80, 893 (1984).
22. X. Y. Huang and T. F. George, J. Phys. Chem. 88, 4801 (1984).
23. X. Y. Huang, K. C. Liu and T. F. George, in Laser-Controlled Chemical Processing of Surfaces, ed. by A. W. Johnson, D. J. Ehrlich and H. R. Scholossber (Elsevier, New York), Mat. Res. Soc. Symp. Prof. 29, 381 (1984).
24. X. Y. Huang, T. F. George and J. Lin, in Coherence and Quantum Optics V, ed. by L. Mandel and E. Wolf (Plenum, New York, 1984), pp. 685-693.

25. J. Lin, X. Y. Huang and T. F. George, Solid State Commun. 47, 63 (1983).
26. X. Y. Huang, K. T. Lee and T. F. George, J. Chem. Phys. 85, 567 (1986).
27. B. R. Mollow, Phys. Rev. 188, 1969 (1969).
28. J. Gersten and A. Nitzan, J. Chem. Phys. 73, 3023 (1980).
29. A. C. Pineda and D. Ronis, J. Chem. Phys. 83, 5330 (1985).
30. H. Metiu, Prog. Surf. Sci. 17, 153 (1984).
31. S. R. J. Brueck and D. J. Ehrlich, Phys. Rev. Lett. 48, 1678 (1982).
32. S. S. Jha, J. R. Kirtley and J. C. Tsang, Phys. Rev. B 22, 3973 (1980).
33. D. Jelski and T. F. George, J. Appl. Phys., submitted.
34. A. Marvin, F. Toigo and V. Celli, Phys. Rev. B 11, 2777 (1975).
35. A. A. Maradudin, in Surface Polaritons, ed. by V. M. Agranovich and D. L. Mills (North-Holland, Amsterdam, 1982), Chapt. 10.
36. D. Agassi and T. F. George, Phys. Rev. B 33, 2393 (1986); Surf. Sci. 172, 230 (1986).
37. P. T. Leung and T. F. George, J. Chem. Phys., in press.

DL/413/83/01
GEN/413-2

TECHNICAL REPORT DISTRIBUTION LIST, GEN

	No. Copies
Office of Naval Research Attn: Code 413 800 N. Quincy Street Arlington, Virginia 22217	2
Dr. Bernard Douda Naval Weapons Support Center Code 5042 Crane, Indiana 47522	1
Commander, Naval Air Systems Command Attn: Code 310C (H. Rosenwasser) Washington, D.C. 20360	1
Naval Civil Engineering Laboratory Attn: Dr. R. W. Drisko Port Hueneme, California 93401	1
Defense Technical Information Center Building 5, Cameron Station Alexandria, Virginia 22314	12
DTNSRDC Attn: Dr. G. Bosmajian Applied Chemistry Division Annapolis, Maryland 21401	1
Dr. William Tolles Superintendent Chemistry Division, Code 6100 Naval Research Laboratory Washington, D.C. 20375	1
Dr. David Young Code 334 NORDA NSTL, Mississippi 39529	1
Naval Weapons Center Attn: Dr. Ron Atkins Chemistry Division China Lake, California 93555	1
Scientific Advisor Commandant of the Marine Corps Code RD-1 Washington, D.C. 20380	1
U.S. Army Research Office Attn: CRD-AA-IP P.O. Box 12211 Research Triangle Park, NC 27709	1
Mr. John Boyle Materials Branch Naval Ship Engineering Center Philadelphia, Pennsylvania 19112	1
Naval Ocean Systems Center Attn: Dr. S. Yamamoto Marine Sciences Division San Diego, California 91232	1
Dr. David L. Nelson Chemistry Division Office of Naval Research 800 North Quincy Street Arlington, Virginia 22217	1

ABSTRACTS DISTRIBUTION LIST, 056/625/629

Dr. G. A. Somorjai
Department of Chemistry
University of California
Berkeley, California 94720

Dr. J. Murday
Naval Research Laboratory
Surface Chemistry Division (6170)
455 Overlook Avenue, S.W.
Washington, D.C. 20375

Dr. J. B. Hudson
Materials Division
Rensselaer Polytechnic Institute
Troy, New York 12181

Dr. Theodore E. Madey
Surface Chemistry Section
Department of Commerce
National Bureau of Standards
Washington, D.C. 20234

Dr. J. E. Demuth
IBM Corporation
Thomas J. Watson Research Center
P.O. Box 218
Yorktown Heights, New York 10598

Dr. M. G. Lagally
Department of Metallurgical
and Mining Engineering
University of Wisconsin
Madison, Wisconsin 53706

Dr. R. P. Van Duyne
Chemistry Department
Northwestern University
Evanston, Illinois 60637

Dr. J. M. White
Department of Chemistry
University of Texas
Austin, Texas 78712

Dr. D. E. Harrison
Department of Physics
Naval Postgraduate School
Monterey, California 93940

Dr. W. Kohn
Department of Physics
University of California, San Diego
La Jolla, California 92037

Dr. R. L. Park
Director, Center of Materials
Research
University of Maryland
College Park, Maryland 20742

Dr. W. T. Peria
Electrical Engineering Department
University of Minnesota
Minneapolis, Minnesota 55455

Dr. Keith H. Johnson
Department of Metallurgy and
Materials Science
Massachusetts Institute of Technology
Cambridge, Massachusetts 02139

Dr. S. Sibener
Department of Chemistry
James Franck Institute
5640 Ellis Avenue
Chicago, Illinois 60637

Dr. Arnold Green
Quantum Surface Dynamics Branch
Code 3817
Naval Weapons Center
China Lake, California 93555

Dr. A. Wold
Department of Chemistry
Brown University
Providence, Rhode Island 02912

Dr. S. L. Bernasek
Department of Chemistry
Princeton University
Princeton, New Jersey 08544

Dr. P. Lund
Department of Chemistry
Howard University
Washington, D.C. 20059

ABSTRACTS DISTRIBUTION LIST, 056/625/629

Dr. F. Carter
Code 6132
Naval Research Laboratory
Washington, D.C. 20375

Dr. Richard Colton
Code 6112
Naval Research Laboratory
Washington, D.C. 20375

Dr. Dan Pierce
National Bureau of Standards
Optical Physics Division
Washington, D.C. 20234

Dr. R. Stanley Williams
Department of Chemistry
University of California
Los Angeles, California 90024

Dr. R. P. Messmer
Materials Characterization Lab.
General Electric Company
Schenectady, New York 22217

Dr. Robert Gomer
Department of Chemistry
James Franck Institute
5640 Ellis Avenue
Chicago, Illinois 60637

Dr. Ronald Lee
R301
Naval Surface Weapons Center
White Oak
Silver Spring, Maryland 20910

Dr. Paul Schoen
Code 5570
Naval Research Laboratory
Washington, D.C. 20375

Dr. John T. Yates
Department of Chemistry
University of Pittsburgh
Pittsburgh, Pennsylvania 15260

Dr. Richard Greene
Code 5230
Naval Research Laboratory
Washington, D.C. 20375

Dr. L. Kesmodel
Department of Physics
Indiana University
Bloomington, Indiana 47403

Dr. K. C. Janda
California Institute of Technology
Division of Chemistry and Chemical Engineering
Pasadena, California 91125

Dr. E. A. Irene
Department of Chemistry
University of North Carolina
Chapel Hill, Northc Carolina 27514

Dr. Adam Heller
Bell Laboratories
Murray Hill, New Jersey 07974

Dr. Martin Fleischmann
Department of Chemistry
Southampton University
Southampton SO9 5NH
Hampshire, England

Dr. John W. Wilkins
Cornell University
Laboratory of Atomic and Solid State Physics
Ithaca, New York 14853

Dr. Richard Smardzewski
Code 6130
Naval Research Laboratory
Washington, D.C. 20375

Dr. H. Tachikawa
Chemistry Department
Jackson State University
Jackson, Mississippi 39217

ABSTRACTS DISTRIBUTION LIST, 056/625/629

Dr. R. G. Wallis
Department of Physics
University of California
Irvine, California 92664

Dr. D. Ramaker
Chemistry Department
George Washington University
Washington, D.C. 20052

Dr. J. C. Hemminger
Chemistry Department
University of California
Irvine, California 92717

Dr. T. F. George
Chemistry Department
University of Rochester
Rochester, New York 14627

Dr. G. Rubloff
IBM
Thomas J. Watson Research Center
P.O. Box 218
Yorktown Heights, New York 10598

Dr. Horia Metiu
Chemistry Department
University of California
Santa Barbara, California 93106

Dr. W. Goddard
Division of Chemistry
California Institute of Technology
Pasadena, California 91125

Dr. J. T. Keiser
Department of Chemistry
University of Richmond
Richmond, Virginia 23173

Dr. R. W. Plummer
Department of Physics
University of Pennsylvania
Philadelphia, Pennsylvania 19104

Dr. E. Yeager
Department of Chemistry
Case Western Reserve University
Cleveland, Ohio 41106

Dr. N. Winograd
Department of Chemistry
Pennsylvania State University
University Park, Pennsylvania 16802

Dr. Roald Hoffmann
Department of Chemistry
Cornell University
Ithaca, New York 14853

Dr. A. Steckl
Department of Electrical and
Systems Engineering
Rensselaer Polytechnic Institute
Troy, NewYork 12181

Dr. G. H. Morrison
Department of Chemistry
Cornell University
Ithaca, New York 14853

Dr. P. Hansma
Physics Department
University of California
Santa Barbara, California 93106

Dr. J. Baldeschwieler
California Institute of Technology
Division of Chemistry
Pasadena, California 91125

ABSTRACTS DISTRIBUTION LIST, 056/625/629

Dr. J. E. Jensen
Hughes Research Laboratory
3011 Malibu Canyon Road
Malibu, California 90265

Dr. J. H. Weaver
Department of Chemical Engineering
and Materials Science
University of Minnesota
Minneapolis, Minnesota 55455

Dr. W. Goddard
Division of Chemistry
California Institute of Technology
Pasadena, California 91125

Dr. A. Reisman
Microelectronics Center of North Carolina
Research Triangle Park, North Carolina
27709

Dr. M. Grunze
Laboratory for Surface Science and
Technology
University of Maine
Orono, Maine 04469

Dr. J. Butler
Naval Research Laboratory
Code 6115
Washington D.C. 20375

Dr. L. Interante
Chemistry Department
Rensselaer Polytechnic Institute
Troy, New York 12181

Dr. Irvin Heard
Chemistry and Physics Department
Lincoln University
Lincoln University, Pennsylvania 19352

Dr. K.J. Klaubunde
Department of Chemistry
Kansas State University
Manhattan, Kansas 66506

Dr. W. Knauer
Hughes Research Laboratory
3011 Malibu Canyon Road
Malibu, California 90265

Dr. C. B. Harris
Department of Chemistry
University of California
Berkeley, California 94720

Dr. F. Kutzler
Department of Chemistry
Box 5055
Tennessee Technological University
Cookesville, Tennessee 38501

Dr. D. DiLella
Chemistry Department
George Washington University
Washington D.C. 20052

Dr. R. Reeves
Chemistry Department
Renssaeler Polytechnic Institute
Troy, New York 12181

END

DTIC

9-86